TEST Engineering & Management

March - April 2020
ISSN: 0193-4120 Page No. 4172 - 4179

Analysis of Loss according to the Ferromagnetic Materials of an Induction Heater for Electric Vehicles

Byoung-Wook Jo[1], Byeong-Chul Lee[2], Ki-Chan Kim[*3]
[1,2]Master degree, Dept. of Electrical Engineering, Hanbat National University, Deaieon, 305-716, South Korea.
[*3]Professor, Dept. of Electrical Engineering, Hanbat National University, Deaieon, 305-716, South Korea.
jbwjbwjbw@naver.com[1], soonia0000@naver.com[2], kckim@hanbat.ac.kr[*3]

Article Info
Volume 83
Page Number: 4172 - 4179
Publication Issue:
March - April 2020

Abstract
: Electric vehicles (EVs) are required to have an independent heater system capable of heating the battery and the room. The heat sources of the induction heater are the copper and core losses. If an induction heater is generated from a high copper loss, the insulation level of the coil increases, which will cause a price increase. Therefore, it is important to increase the core loss generated from the work piece (WP, heating element). Ferromagnetic materials are mainly selected for the WP of induction heaters. The core loss is the sum of the hysteresis, eddy current, and excess losses generated from the ferromagnetic materials in a time-varying magnetic field. The hysteresis loss is proportional to the hysteresis loop. This loop is determined by the B-H curve, coercive force, and residual flux. The eddy current loss is determined by the induced voltage in the WP, and the excess loss is determined by the harmonics of the current.

System: In this paper, three ferromagnetic materials with different BH curves, residual magnetic fluxes, and coercive forces were selected. Also, the loss characteristics of the three ferromagnetic materials were analyzed through the modeling of the parallelogram hysteresis loop and finite element method (FEM) simulation. Finally, the analysis results were verified through experiments..

Article History
Article Received*: 24 July 2019*
Revised*: 12 September 2019*
Accepted*: 15 February 2020*
Publication*: 26 March 2020*

Keywords: *B-H curve, coercive force, core loss, hysteresis loop, induction heater, work piece.*

1. Introduction

Due to the exhaust gas regulations, the global automobile market is shifting from internal-combustion-engine vehicles to electric vehicles (EVs). In EVs, unlike in internal-combustion-engine vehicles, the waste heat of the engine cannot be used, and the battery efficiency rapidly deteriorates if the battery does not maintain the proper temperature [1]. As such, EVs are required to have an independent heater system capable of heating the battery and the room [2]. The induction heater is light weight and has a low manufacturing cost due to its simple insulation structure. In addition, as the induction heater is operated near the resonance point, the heating rate is fast [3-10]. Therefore, the induction heater will be a good heater for EVs. The heat sources of the induction heater are the copper and core losses [11]. If an induction heater is generated from a high copper loss in a coil, the insulation level of the coil increases, which will cause a price increase. Therefore, it is important to increase the core loss generated from the work piece (WP, heating element). Ferromagnetic materials are mainly selected for the WP of induction heaters. The core loss is the sum of the hysteresis, eddy current, and excess losses generated from the ferromagnetic materials in a time-varying magnetic field [12]. The hysteresis loss is proportional to the hysteresis loop. This loop is determined by the B-H curve, coercive force, and residual flux. The eddy current loss is determined by the induced voltage in the WP, and the excess loss is determined by the harmonics of the current. In general, the hysteresis loss is also proportional to the frequency, the eddy current loss is proportional to the square of the frequency, and the excess loss is proportional to 1.5 times the frequency[13],[14]. In this paper, three ferromagnetic materials with different B-H curves, residual magnetic fluxes, and coercive forces were selected. Also, the loss characteristics of the three ferromagnetic materials were analyzed through the modeling of the parallelogram hysteresis loop and FEM simulation. Finally, the analysis results were verified through experiments.

2. Analysis of the System of Induction Heaters

2.1 Structure of induction heaters

Fig. 1 shows the structure of an induction heater. As shown in Fig. 1(a), an induction heater is made up of a coil, the WP, the case, a bobbin, and a header. The alternating magnetic field is generated by flowing AC current through a coil, and the core loss is generated by the alternating magnetic field in the WP. In addition, the bobbin and header, respectively, shape the coil and the WP, and the case shields the leakage flux. The case is also configured in such a way that the coolant receives heat from the WP and heats the battery and the room. As shown in Fig. 1(b), two-dimensional finite element method (2D FEM) simulation rather than three-dimensional FEM (3D FEM) simulation was performed to reduce the simulation time. Similarly, the analysis was conducted leaving only the WP and a coil, which are the main factors in the analysis of the electromagnetic field of an induction heater.

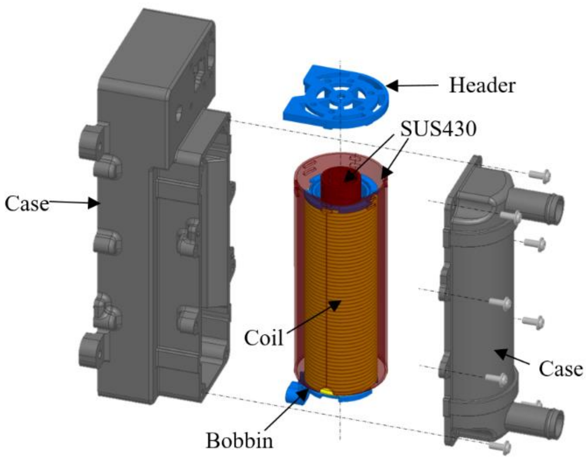

(a)

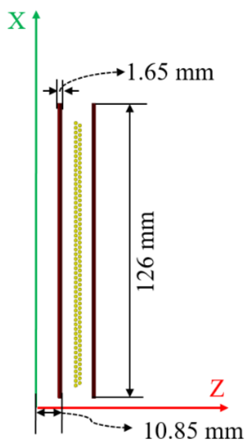

(b)

Figure 1. Structure of an induction heater: (a) 3D structure of an induction heater; and (b) structure of the 2D FEM simulation model.

2.2 Structure of induction heaters

Fig. 2(a) shows the H-bridge circuit. The maximum voltage of the EV battery is 510 Vdc. The maximum voltage applied to an induction heater is limited to 360 Vrms. Fig. 2(b) shows the gate signal of IGBT. The input frequency is set to 42 kHz, and a coil is applied to the sinusoidal current through the RLC inverter circuit, as shown in Fig. 2(b).

TEST Engineering & Management
March - April 2020
ISSN: 0193-4120 Page No. 4172 - 4179

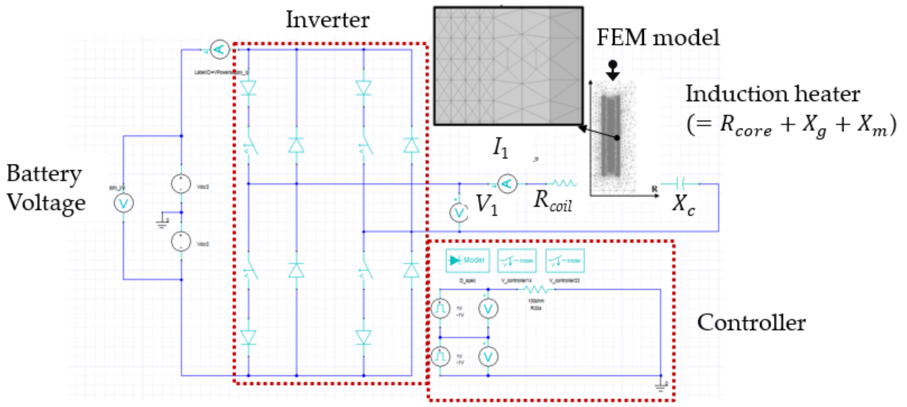

(a)

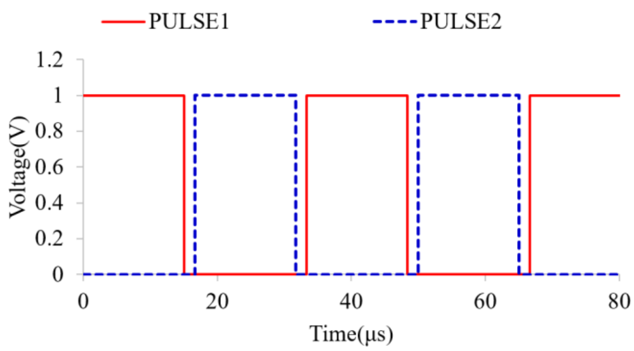

(b)

Figure 2. RLC circuit and gate signal of H-bridge: (a) H-bridge RLC circuit; and (b) gate signal of IGBT.

2.3 Equivalent circuit of induction heaters

Fig. 3 shows the magnetic equivalent circuit and phase diagram of an induction heater. The flux linkage of the induction heater is the sum of the flux linking the WP and the flux linking in the air, as shown in Fig. 3. Equations (1), (2), (3), and (4) represent the flux of the WP, the flux of the air gap, the reactance of the WP, and the reactance of the air gap, respectively.

$$\phi_m = \frac{P_m}{P_m + P_g}\phi_t \tag{1}$$

$$\phi_g = \frac{P_g}{P_m + P_g}\phi_t \tag{2}$$

$$X_m = \omega L_m \tag{3}$$

$$X_g = \omega L_g \tag{4}$$

where P_g and P_m represent the permeance of the air gap and the permeance of the WP, respectively. Fig. 4 shows the equivalent circuit of an induction heater. Equations (5) and (6) represent the current applied to a coil and the power factor, respectively. In terms of energy, the power factor is important because the induction heater has 100% efficiency. When the reactance is offset by that of the capacitor, as shown in equations (5) and (6), only the core loss resistance and the resistance of a coil component exist in the impedance. Therefore, the current is maximized alongside the output.

$$I_1 = \frac{V_1}{\sqrt{(R_{coil} + R_{core})^2 + (X_g + X_m - X_c)^2}} \tag{5}$$

$$\cos\theta = \frac{R_{coil} + R_{core}}{\sqrt{(R_{coil} + R_{core})^2 + (X_g + X_m - X_c)^2}} \tag{6}$$

March - April 2020
ISSN: 0193-4120 Page No. 4172 - 4179

where R_{coil}, R_{core}, X_c, and V_1 are the resistance of a coil, core loss resistance, reactance of capacitance, and voltage applied to a coil, respectively.

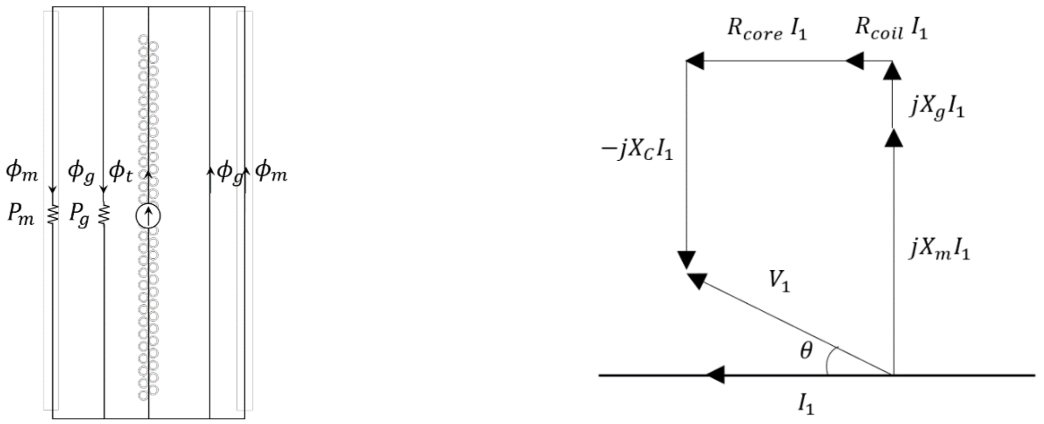

(a) (b)

Figure 3. Magnetic equivalent circuit and phase diagram of an induction heater: (a) magnetic equivalent circuit; and (b) phase diagram.

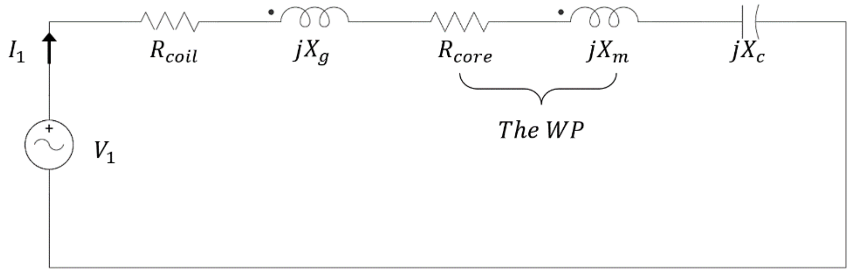

Figure 4. Equivalent circuit of an induction heater.

Fig. 5 shows the B-H curve of the SUS 430-equivalent circuit of an induction heater. Equations (7) and (8) represent the skin depth and flux density of the WP, respectively. A coil of an induction heater operated at a high frequency is used with a Litz wire to reduce the proximity and skin effect. The WP, on the other hand, is operated at high permeability and frequency, as shown in Fig. 5, which is larger than the copper loss.

$$\delta = \frac{1}{\sqrt{\pi f \sigma \mu}} \quad (7)$$

$$B_m = \mu_0 \mu_r H_m \quad (8)$$

where σ, μ, and Hm are the relative permeability, conductivity, and magnetic field of the WP.

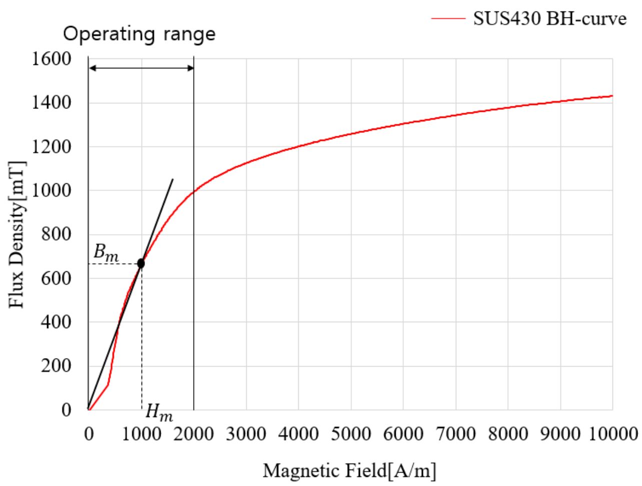

Figure 5. B-H curve of SUS 430.

3. Analysis of the Heat Source of Induction Heaters

Fig. 6 show the generation process of eddy current in the WP and the modeling of the parallelogram hysteresis loop. Equation (9) represents the general core loss for electrical steel. K_h, K_c, and K_e, are the hysteresis, eddy current, and excess loss coefficients, respectively. The hysteresis loss coefficient is related to the hysteresis loop area, the eddy current loss coefficient is related to the induced voltage in the WP and the core loss resistance, and the excess loss coefficient is related to the harmonics of the current. Induction heaters, however, are close to sinewaves, so the coefficient value is almost zero. The parallelogram hysteresis loop is derived based on the measured B-H curve, coercive force, and residual flux. The first step is the drawing of a tangent line at each point before and after saturation on the measured B-H curve, as shown in Fig. 6(b). The second step is the drawing of the same tangent line before saturation on both sides of the measured coercive force. The third step is the connection of the four intersections of the tangent lines drawn earlier. This is a parallelogram hysteresis loop.

$$\text{Core loss} = K_h f(B_m)^2 + K_c(fB_m)^2 + K_e(fB_m)^{1.5} \quad (9)$$

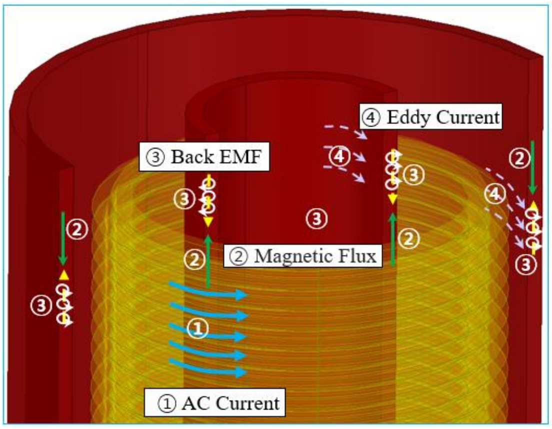

(a)

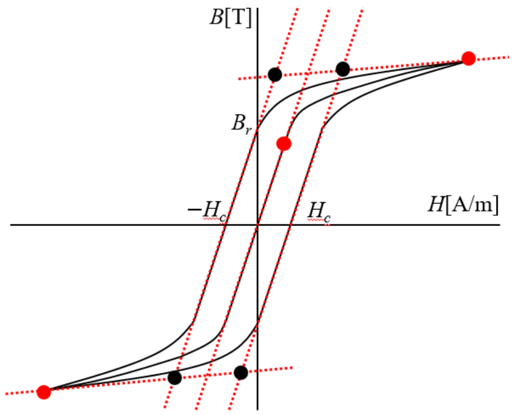

(b)

Figure 6. Generation process of eddy current in the WP.

Fig. 7 shows the parallelogram hysteresis loop from B_m=0.2[T] to B_m=1.55[T]. These loops were drawn using the same method described earlier. Fig. 8 shows the three parallelogram hysteresis loops at B_m=1[T] . Model B represents the B-H curve and parallelogram hysteresis loop of SUS 430. The coercive force and saturated flux density of model A are 10% higher than those of model B, and those of model C are 10% lower. As shown in Fig. 8, the hysteresis loop of model A is about 20% larger than that of model B, and the hysteresis loop of model C is about 20% smaller. Table 1 compares the model A, B, and C core losses. The operating frequency was the same (42 kHz).

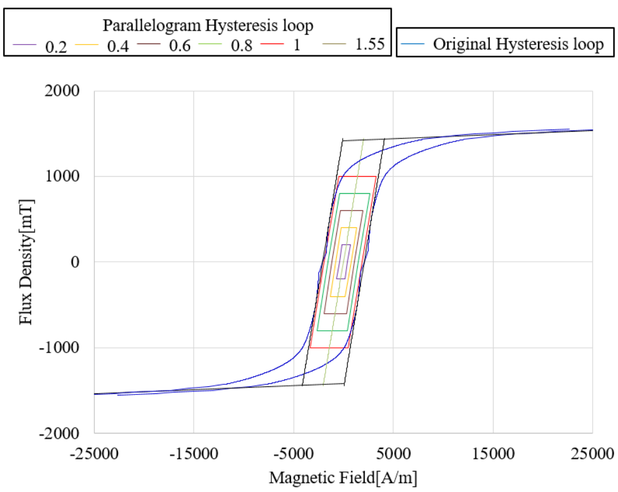

Figure 7. Parallelogram hysteresis loop from B_m=0.2[T] to B_m=1.55[T].

TEST Engineering & Management

March - April 2020
ISSN: 0193-4120 Page No. 4172 - 4179

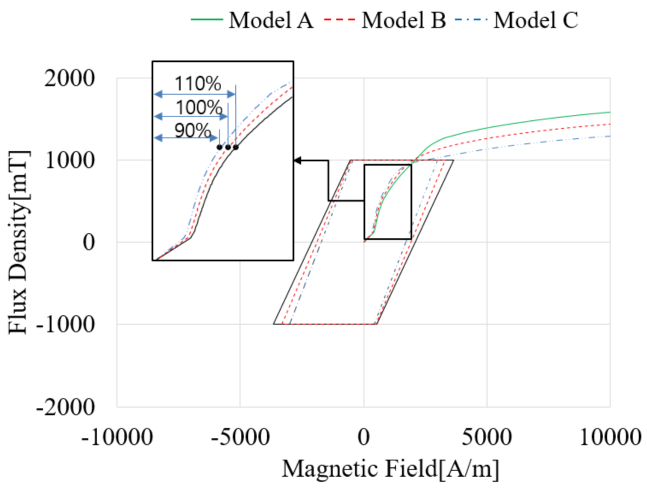

Figure 8. Three parallelogram hysteresis loops at B_m=1[T]

Fig. 9 and Table 1 show the core loss distribution per model obtained through 2D FEM simulation, and compare the model A, B, and C losses. Model A has the lowest initial permeability of the B-H curve, resulting in the lowest core loss resistance and the highest current. It also has the largest hysteresis loop area. Therefore, model A has the highest core loss, as shown in Fig. 10. The hysteresis loop of each of the three models differs by 20% from those of the other models, but because they operate at a high frequency, the eddy current loss proportional to the square of the frequency is greater than the hysteresis loop proportional to the frequency. As such, the core loss increased by 3.6 and 4.3%.

Table 1. Comparison of the model A, B, and C losses

Spec.	Model A	Model B	Model C	Unit
Cap.	0.432	0.432	0.432	μF
Voltage	353.04	355.35	354.50	V_{rms}
Current	21.86	21.24	20.67	A_{rms}
Input	7715.96	7547.63	7326.86	W
Core loss	6695.76	6415	6193.88	W
Copper loss	76.43	72.18	68.35	W
Output	6772.19	6487.18	6262.23	W
PF	0.878	0.859	0.854	-

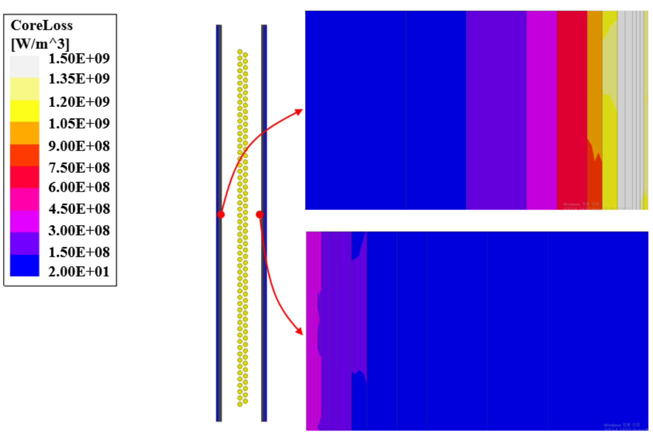

(a)

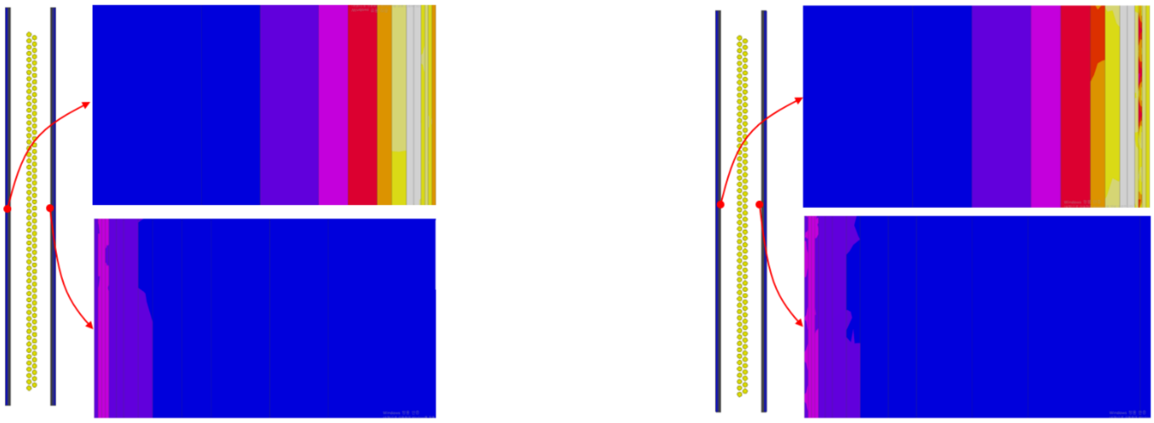

(b) (c)

Figure 9. Core loss distribution per model: (a) model A; (b) model B; and (c) model C..

4. Conclusion

In this study, the core loss characteristics when the coercive force, residual magnetic flux, and B-H curve were changed with a ferromagnetic material (SUS 430) were analyzed. As the analysis result, it was found that model A with a small initial permeability but a high saturation level, and hysteresis loop is the most suitable material for induction heaters. However, the hysteresis loop of each of the three models differs by 20% from those of the other models, but because they operate at a high frequency, the eddy current loss proportional to the square of the frequency is greater than the hysteresis loop proportional to the frequency. As such, the core loss increased by 3.6 and 4.3%.

Acknowledgment

This work was supported by the National Research Foundation of Korea(NRF) grant funded by the Korea government(MSIT) (No. NRF-2019R1F1A1058504).

References

[1] A. Emadi, K. Rajashekara, S. S. Williamson, and S. M. Lukic, "Topological overview of hybrid electric and fuel cell vehicular power system architectures and configurations," IEEE Trans. Veh. Technol., Vol. 54, No. 3, pp. 763–770, May 2005.

[2] A. Boadi, Y. Tsuchida, T. Todaka and M. Enokizono, "Designing of suitable construction of high-frequency induction heating coil by using finite-element method," IEEE Trans. Magn., Vol.41, No.10, pp.4048-4050, 2005.

[3] H. Kagimoto, D. Miyagi, N. Takahashi, N. Uchida, and K. Kawanaka, "Effect of Temperature Dependence of Magnetic Properties on Heating Characteristics of Induction Heater," IEEE Trans. Magn., Vol.46, No.8, pp.3018-3021, 2010.

[4] Jesús Acero, Claudio Carretero, Rafael Alonso and José M. Burdio, "Quantitative Evaluation of Induction Efficiency in Domestic Induction Heating Applications," IEEE Trans. Magn., Vol.49, No.4, pp.1382-1389, 2013.

[5] S.M. Jang, S. K. Cho, S. H, Lee, H. W. Cho and H. C. Park , "Thermal analysis of induction heating roll with heat pipes," IEEE Trans. Magn., Vol.39, No.5, pp.3244-3246, 2003.

[6] T. Wang, P. Zheng, Q. Zhang and S. Cheng, "Design characteristics of the induction motor used for hybrid electric vehicle," IEEE Trans. Magn., Vol.41, No.1, pp.505-508, 2005.

[7] Z. Keyi, L. Bin, L. Zhiyuan, C. Shukang, and Z. Ruiping, "Inductance Computation Consideration of Induction Coil Launcher," IEEE Trans. Magn., Vol.45, No.1, pp.336-340, 2009.

[8] H. Kurose, D. Miyagi, N. Takahashi, N. Uchida and K. Kawanaka,"3-D Eddy Current Analysis of Induction Heating Apparatus Considering Heat Emission, Heat Conduction, and Temperature

Dependence of Magnetic Characteristics," IEEE Trans. Magn., Vol. 45, No.3 pp.1847-1850, 2009.
[9] S. Kawashima, T. Ishigohka, A. Ninomiya, and M. Furuse, "Power System Voltage Stabilizer Using LC Resonance Circuit With Superconduction Coil and Capacitor," IEEE Trans. Magn., Vol.19, No.3, 2009.
[10] Oscar Lucia, JosÉ M. Burdio, Ignacio Millan, JesÚs Acero and Diego Puyal, "Load-Adaptive Control Algorithm of Half-Bridge Series Resonant Inverter for Domestic Induction Heating," IEEE Trans. Magn., Vol.56, No.8, pp.3106-3116, 2009.1
[11] Nikolaos. Tsopelas and Nicolaos J. Siakavellas, "Influence of Some Parameters on the Effectiveness of Induction Heating," IEEE Trans. Magn., Vol.44, No.12, pp.4711-4720, 2008.2
[12] Yunkai Huag, Jianning Dong, Jianguo Zhu, and Youguang Gud, "Core Loss Modeling for Permanent-Magnet Motor Based on Flux Varization Locus and Finite-Element Method" IEEE Trans. Magn., Vol.48, No.2, pp.1023-1026, 2012.
[13] Junquan Chen, Dong Wang, Siwei Cheng, Yapeng Jiang, Xuan Teng, and Yunjun Guo, "Influence of DC-Biased Magnetic Induction on Magnetic Property of Silicon Steel," IEEE Trans. Magn., Vol.55, No.5, 2019.
[14] Seok-Hyun Yo, Dong-Jin Park, and Ki-Chan Kim, "Heat Source Analysis of an Induction Heater for an Electric Vehicle," IEEE Trans. Magn., Vol.53, No.6, 2017.